JACS
JOURNAL OF THE AMERICAN CHEMICAL SOCIETY
Communication
pubs.acs.org/JACS

Foldecture as a Core Material with Anisotropic Surface Characteristics

Sung Hyun Yoo,[†] Taedaehyeong Eom,[‡] Sunbum Kwon,[†] Jintaek Gong,[†] Jin Kim,[§] Sung June Cho,[∥] Russell W. Driver,[†] Yunho Lee,[§] Hyungjun Kim,*[,‡] and Hee-Seung Lee*[,†]

[†]Molecular-Level Interface Research Center, Department of Chemistry, [‡]Graduate School of EEWS, and [§]Department of Chemistry, KAIST, Daejeon 305-701, Korea

[∥]Department of Applied Chemical Engineering, Chonnam National University, Gwangju 500-757, Korea

Supporting Information

ABSTRACT: The synthesis of microscale, polyhedrally shaped, soft materials with anisotropic surface functionality by a bottom-up approach remains a significant challenge. Herein we report a microscale molecular architecture (foldecture) with facet-dependent surface characteristics that can potentially serve as a well-defined catalytic template. Rhombic rod shaped foldectures with six facets were obtained by the aqueous self-assembly of helical β-peptide foldamers with a C-terminal carboxylic acid. An analysis of the molecular packing by X-ray diffraction revealed that carboxylic acid groups were exposed exclusively on the two (001) rhombic facets due to antiparallel packing of the helical peptides. A surface energy calculation by molecular dynamics simulation was performed to provide a plausible explanation for the development of anisotropy during foldecture formation. The expected facet-selective surface properties of the foldecture were experimentally confirmed by selective deposition of metal nanoparticles on the (001) facets, leading to a new class of sequentially constructed, heterogeneous "foldecture core" materials.

The design and synthesis of giant, protein-like molecular assemblies from peptidic materials *in a flask* remains a significant challenge in light of the marvelous topological complexity as well as functional anisotropy realized in biological architectures such as viral capsids and intracellular microcompartments.[1] Attempts to understand the self-assembly process through a "bottom-up" analysis of the interactions between individual constituents have attracted considerable interest as a way to engineer macroscopic morphologies, albeit with only a few successful examples using highly aromatic compounds.[2]

Peptides are particularly useful building blocks for the development of new biocompatible materials due to their catalytic activities and molecular recognition abilities. However, the repertoire of morphologies reported for short α-peptidic scaffolds has been limited to relatively simple isotropic shapes,[3] primarily because α-peptides can adopt multiple low-energy conformations in both the solution and solid states.[4] However, β-peptide foldamers, which are known to adopt well-defined and predictable secondary structures in solution, have proven to be excellent building blocks for higher-order supramolecular structures.[5] In addition, foldamers with precisely situated functional groups can form supramolecular assemblies with enzyme-like catalytic activity.[6]

Our group has recently reported a new class of microscale materials with unprecedented three-dimensional (3D) shapes derived from the self-assembly of helical peptide foldamers, which we have termed foldectures (foldamers + architectures).[7] Foldectures exhibit discrete and diverse instances of morphologies with high crystallinity as well as unrivaled uniformity in terms of their shape and size. These highly desirable structural properties allow for the design of biocompatible, microscale hierarchical assemblies with polyhedral shapes. If the necessary functional groups were displayed with spatial periodicity on the surface of certain facets of a well-defined structural framework, this "surface-functionalized foldecture" would serve as a core material ready for further structural elaboration or could be employed as a huge protein-like catalyst. Foldectures that selectively display oxygen-rich functionalities are particularly attractive as core materials for the development of spatioselective biomineral composites, a challenging area in which there has been limited success.[8]

In order to design 3D microscale architectures with functional anisotropy, several factors must be considered. First, an appreciation of the secondary structure of the foldamer building block is necessary because the conformation and functional groups of the foldamer will be directly reflected in the physical properties of the resulting foldecture. Second, an in-depth study of the self-assembly process is required to understand the mechanism of foldecture morphogenesis at the molecular level. Foldecture formation is influenced by both molecular level interactions between foldamers and interactions with the environment (e.g., water molecules or additives), although no theoretical studies have yet been performed. Moreover, there remains the unanswered question as to how we can unambiguously ascertain the presence of functional groups on each facet of the foldecture because direct surface analysis of foldectures is hampered by their microscale dimensions. Although we are able to analyze the molecular packing motif of foldectures through powder X-ray diffraction (PXRD),[7b,c] it is essential to obtain direct evidence correlating the orientation of individual foldamer helical axes with foldecture morphology.

Received: October 22, 2014
Published: January 30, 2015

DOI: 10.1021/ja510840v
J. Am. Chem. Soc. 2015, 137, 2159−2162

On the basis of these considerations, we envisioned the design of a new class of foldecture in which functional groups are selectively displayed only on specific facets and subsequently elaborated to form composite "foldecture core" materials. Herein we report rhombic rod-shaped foldectures with anisotropic, facet-specific surface properties from the self-assembly of 12-helical β-peptide foldamers with a *C*-terminal carboxylic acid moiety. Specific facets displaying carboxylic acid functional groups were assigned by X-ray diffraction techniques in combination with a surface energy calculation by molecular dynamics simulation. The facet-specific physical properties of foldectures were confirmed by facet-selective nanoparticle deposition experiments.

A desired foldecture with anisotropic characteristics could be obtained through the self-assembly of *trans*-(*S*,*S*)-2-amino-cyclopentanecarboxylic acid (ACPC) hexamer with a *C*-terminal carboxylic acid moiety, **1** (Figure 1a), which was easily prepared by the debenzylation of the known 12-helical hexapeptide.[7b,d] In **1**, the hydrophobic cyclopentane rings and the Boc group are displayed on the helical periphery and the *N*-terminus of the helix, respectively (Figure 1a). The self-assembly of **1** by our standard protocol (see Supporting Information) was performed in aqueous solution in both absence and presence of P123 (Pluronic P123, (ethylene glycol)$_{20}$-(propylene glycol)$_{70}$-(ethylene glycol)$_{20}$) surfactant (8 g L^{-1}), to provide two distinct types of 3D shapes, a rhombic plate ($\mathbf{F_1}$) and a rhombic rod ($\mathbf{F_2}$), respectively (Figure 1b). Scanning electron microscopy (SEM) analysis revealed that $\mathbf{F_1}$ is a C_i-symmetrical thin plate with two rhombic facets, which have interior angles of ca. 108° and 72°. The width and thickness are ca. 2−3 μm and 200 nm, respectively ($\mathbf{F_1}$, Figure 1c). Foldecture $\mathbf{F_2}$ has a rhombic rod shape with six facets (that is, four rectangular facets and two rhombic facets) and sharp edges with lengths of ca. 3 and 0.6 μm (Figure 1d). Interestingly, both $\mathbf{F_1}$ and $\mathbf{F_2}$ have rhombic facets with identical internal angles. The nicked edges of $\mathbf{F_1}$, which contrast with the smooth edges of $\mathbf{F_2}$, are consistent with $\mathbf{F_1}$ entering a dendritic growth regime.[9] The difference in growth rates between $\mathbf{F_1}$ and $\mathbf{F_2}$ may result from surfactant adsorption onto nascent foldectures, thereby retarding the association of building blocks. The relationship between $\mathbf{F_1}$ and $\mathbf{F_2}$ was examined by self-assembly studies in different P123 concentrations (Figure S2). Longitudinal growth along the direction perpendicular to the rhombic facets was favored by increasing P123 concentration. A concomitant reduction in the area of the rhombic facets was observed, although the internal angles were preserved. We attribute the formation of the rhombic rod shapes of $\mathbf{F_2}$ to the preferential interaction of P123 surfactant with the lateral, rectangular facets as illustrated in Figure 1b.

To investigate the molecular packing motif of $\mathbf{F_2}$ in detail, powder X-ray diffraction patterns were obtained from the SPring-8 synchrotron. An analysis of the PXRD data by pattern indexing, Le Bail fitting, and Rietveld refinement (Supporting Information) revealed that $\mathbf{F_2}$ has an orthorhombic crystal system and a $P2_12_12_1$ space group, with cell parameters of a = 11.2462(4) Å, b = 15.4783(5) Å, c = 25.0742(6) Å, and $\alpha = \beta = \gamma = 90°$, and a cell volume of 4364.72 Å^3 (Figure 2). The helical axes of the constituent foldamers are aligned along the *c*-axis of the unit cell, with two pairs of intermolecular hydrogen bonds ((C═O)$_{i+4}$ → (H−N)$_j$ and (C−O)$_{i+6}$ → (H−N)$_{j+1}$) connecting helices in a zigzag-type network (Figure 2b). At the same time, adjacent foldamer helices are arranged in a head-to-tail fashion (Figure 2a,b), thus creating a laminar, antiparallel stacking motif that presents the *C*-terminal carboxylic acid groups parallel to the *ab* plane of the unit cell (shown as the dashed line and the yellow rhombus in Figure 2b,c, respectively).This structural analysis suggested strongly that the two rhombic facets of $\mathbf{F_2}$ (as well as $\mathbf{F_1}$) can be assigned as (001) plane.[10] This result implies that the carboxylic acid groups are primarily displayed on the rhombic (001) facets that are perpendicular to the longitudinal axis of $\mathbf{F_2}$, while the hydrophobic helical faces of the foldamers are mainly exposed on the rectangular facets. Thus, we can tentatively assign the (110) and (−110) planes as rectangular facets and (001) as rhombic facets. We also found that the molecular packing modes of $\mathbf{F_1}$ and $\mathbf{F_2}$ are essentially identical (Figure S5). It was anticipated

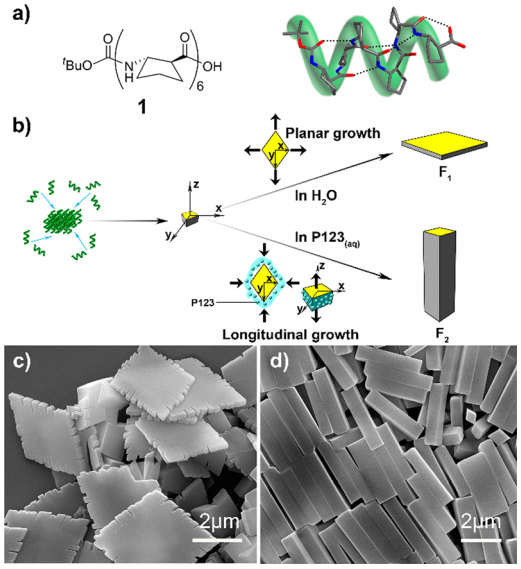

Figure 1. (a) Chemical structure of BocNH-ACPC$_6$-OH, **1** (left), and its single crystal X-ray structure overlapped with a green helical representation (right, the intramolecular hydrogen bonds are depicted as dotted lines; hydrogen atoms are omitted for clarity). (b) Schematic representation of foldecture formation. (c,d) SEM images of the foldectures of **1** prepared from (c) distilled water ($\mathbf{F_1}$) and (d) 8 g L^{-1} of aqueous P123 solution ($\mathbf{F_2}$).

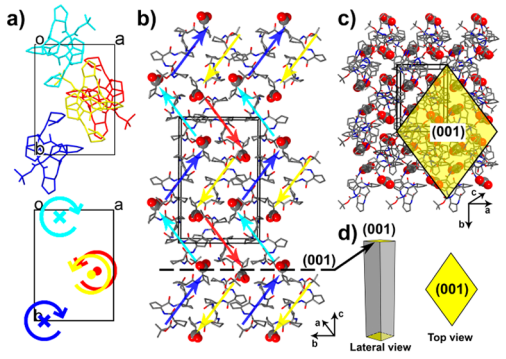

Figure 2. (a) Molecular packing motif of foldecture $\mathbf{F_2}$ in the unit cell. A view along the *c*-axis is shown at top and the helical handedness of individual foldamers at bottom. (b) Molecular network viewed along the *a*-axis. Carboxylic acid moieties are depicted as space-filling models. Colored arrows reflect the directions (N to C) of individual helices. The dashed line representing the (001) plane indicates the rhombic faces in panels c and d. (c) A molecular network viewed along the *c*-axis is displayed, on which a yellow rhombus representing the (001) plane and confined by (110) and (−110) is superimposed. (d) The assigned (001) face of $\mathbf{F_2}$ is illustrated.

DOI: 10.1021/ja510840v
J. Am. Chem. Soc. 2015, 137, 2159−2162

that the unique molecular packing mode would create anisotropic macroscopic surface properties in the foldecture.

On the basis of the PXRD analysis, we envisioned that the preferential binding of surfactant molecules to the rectangular facets of the nascent foldecture, which is responsible for the shape evolution from $\mathbf{F}_1$ to $\mathbf{F}_2$ (as illustrated in Figure 1b), could be further investigated by a theoretical consideration of the relative surface energies of each facet of the foldecture. That is, the anisotropic shape of the foldecture likely originates from the differences in surface energy between facets. This assumption is supported by earlier studies in the literature. (1) In the case of crystal growth under thermodynamic control, minimization of the total surface energy is the major determinant of shape.[11] (2) In studies of inorganic nanostructures, a wide variety of surfactants can adsorb onto specific facets of seeds to change the surface energy levels unequally and thereby influence crystal morphogenesis.[12] Similarly, shape control of the foldecture would be regulated by the differences in surface energies of individual facets.

Thus, the determination of the surface energy of each facet is crucial to understand the shape formation of foldectures. The surface energy (E_{surf}) was calculated by molecular dynamics (MD) simulations:

$$E_{surf} = \frac{\langle E_{slab}\rangle - N\langle E_{bulk}\rangle}{2A}$$

where E_{slab} is the energy of the surface slab consisting of N repeating units, E_{bulk} is the energy of the bulk structure per unit cell, A is the surface area, and the brackets denote the ensemble average calculated from MD simulation trajectories. Intermolecular interactions are described using DREIDING force field (FF) parameters[13] coupled with atomic point charges derived using the charge equilibration method (QEq),[14] which reproduces the experimental cell parameters of the single crystal of **1** (Table S1). Using surface slab models with an additional ~50 Å of vacuum above the surface (which consists of 3840 atoms; Figure S6), we conducted canonical ensemble simulations at 300 K for 2 ns, where the last 1 ns of data was used to determine the equilibrium ensemble average energies. The calculated values of E_{surf} for the (001), (010), (100), and (110) surfaces at 300 K are shown in Table 1. Among all facets considered, the (001) surface

Table 1. Surface Energy (E_{surf}), Surface Stabilization Energy Due to Water Solvation (Δ_{wat}), and the Summation of E_{surf} and Δ_{wat} of Each Surface Orientation; Values Are Computed from the Canonical Ensemble Average of MD Simulations at 300 K

surface orientation	E_{surf} (meV/Å^2)	Δ_{wat} (meV/Å^2)	$E_{surf} + \Delta_{wat}$ (meV/Å^2)
(001)	10.96	−16.14	−5.18
(010)	4.58	−6.93	−2.35
(100)	7.42	−11.27	−3.85
(110)	3.75	−5.61	−1.86

was determined to be the most unstable surface; this is attributed to the cleavage of hydrogen bonds. We found that no hydrogen bond cleavage accompanies the surface formation of (010), (100), and (110) surfaces, of which the (110) surface was determined to have the lowest surface energy. Considering that organic surfactants have a low-dielectric constant of ca. 2−3, the values of E_{surf} computed *in vacuo* are applicable to foldecture growth conditions in the presence of P123 and can thus support our hypothesis that the rhombic rod shape of $\mathbf{F}_2$ results from surfactant simultaneously surrounding the (110) and (−110) faces and also minimizing the surface area of (001).

Aqueous environments provide a high dielectric medium with a dielectric constant of ~80, in which water molecules can interact with dangling hydrogen bonds or carboxylic acid groups on the surface. Using MD simulations, we further examined the surface stabilization energies due to water solvation:

$$\Delta_{wat} = \frac{\langle E_{slab(aq)}\rangle - N_{wat}\langle E_{wat}\rangle - \langle E_{slab(vac)}\rangle}{2A}$$

where $E_{slab(aq)}$ is the energy of the surface slab solvated with N_{wat} water molecules (Table S2 and Figure S7), and E_{wat} is the energy per molecule of bulk water. The value of Δ_{wat} for each surface computed from MD simulations is shown in Table 1 (the flexible three-point charge model[15] is used to describe the water molecules). We found that water molecules preferentially bind to the dangling hydrogen bonds on the (001) surface (Figure 3)

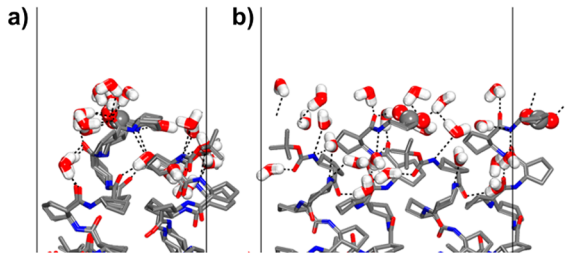

Figure 3. (a) *a*-axis and (b) *b*-axis views of the (001) surface structure taken from the final snapshot of MD simulation showing water stabilization of the surface. For clarity, only water molecules (bold stick) interacting with hydrogen bond on the surface (dashed line) are shown.

and stabilize it with the greatest extent by 16.14 meV/Å^2. In contrast, the (110) surface is stabilized only by 5.61 meV/Å^2. Thus, Δ_{wat} term is sufficient to reverse the energetic preference of the (110) surface over the (001) surface and explain why the (001) facet has the largest area in water solvation conditions. From this surface energy investigation, we can conclude that both intermolecular hydrogen bonding between foldamer building blocks and the facet-specific stabilization by surfactant adhesion play key roles in controlling the morphogenesis of foldectures. These findings are consistent with previous studies on the surfactant-assisted morphogenesis of inorganic nanoparticles and aromatic organic materials.[2,12]

The anisotropic nature of $\mathbf{F}_2$ was imagined to lead to facet-specific physical properties and thus provides an opportunity to design a new class of "foldecture core" composite materials. It is known that the preferential adsorption by surfactant on specific facets results in the selective deposition of metal nanoparticles (NPs) on uncapped surfaces.[16] In analogy, we performed *in situ* Au NP deposition on a naked $\mathbf{F}_2$ core in the presence of P123, using $HAuCl_4 \cdot 3H_2O$ and L-ascorbic acid as a gold precursor and mild reductant, respectively (Figure 4a). The formation of Au (or Pt[17]) NP−foldecture composites was confirmed by visualization with scanning transmission electron microscopy (STEM) and electron dispersive spectroscopy (EDS) (Figure 4b). The resulting Au NPs selectively adhered onto (001) rhombic facets that were expected to poorly adsorb P123. The facet-specific attachment of Au NPs was not observed in a control experiment performed without P123 (Figure S8). Subsequently, we were able to decorate the resulting composite face of $\mathbf{F}_2$ with thiols (Figure 4a) by dispersing Au NP−foldecture composites in an aqueous solution of benzenethiol (BT, 1 mL, 0.05 v/v %) as a Raman-active dye.[18] The unique surface-enhanced Raman scattering

DOI: 10.1021/ja510840v
J. Am. Chem. Soc. 2015, 137, 2159−2162

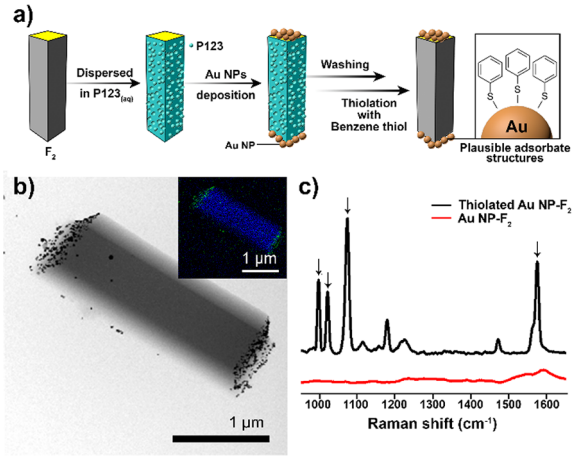

Figure 4. (a) Schematic representation of the facet-selective Au NP deposition and thiolation experiments. (b) STEM image and EDS mapping (inset: blue, C; green, Au) of the Au NP−$\mathbf{F_2}$ composite. (c) SERS spectra of a thiolated Au NP−$\mathbf{F_2}$ composite and an Au NP−$\mathbf{F_2}$ composite in which the characteristic Raman signals of BT are highlighted with arrows.

(SERS) signals of BT (with Raman shifts at 1000, 1025, 1075, and 1575 cm^{-1} as shown Figure 4c) and EDS map image (Figure S10) of the thiolated Au−$\mathbf{F_2}$ composite confirmed the successful facet-specific thiolation. These results suggest that anisotropic metal NP−foldecture composite materials can be utilized as easily synthesized for optical and biochemical applications.

In summary, we have achieved the synthesis of rhombic rod shaped foldectures with anisotropic surface properties by the controlled self-assembly of helical β-peptide foldamers with a *C*-terminal carboxylic acid. An investigation of the molecular packing motif by PXRD analysis, MD surface energy calculations, and NP deposition experiments provided compelling evidence for the dense distribution of carboxylic acid functional groups only on the rhombic facets of the foldecture-leading to facet specific physical properties. We believe this to be the first unambiguous correlation between the spatial orientation of an individual foldamer and the microscale morphology of a polyhedrally shaped peptide assembly. We subsequently harnessed the anisotropic surface characteristics of these unique foldectures to synthesize a new class of metal NP−foldecture composite materials. We expect that this advance in knowledge of the processes that underlie foldecture design and synthesis will make possible the realization of hierarchically assembled,[19] functional foldectures with high levels of topological complexity by facial-selective association using orthogonal adhesives such as DNA.

■ ASSOCIATED CONTENT

Supporting Information

Experimental procedures, additional figures, and characterizations. This material is available free of charge via the Internet at http://pubs.acs.org.

■ AUTHOR INFORMATION

Corresponding Authors

*hee-seung_lee@kaist.ac.kr
*linus16@kaist.ac.kr

Notes

The authors declare no competing financial interest.

■ ACKNOWLEDGMENTS

This research was supported by the National Research Foundation (NRF) of Korea grant funded by Ministry of Science, ICT, and Future Planning (2013R1A2A1A01008358 and 2013M3A6B1078884).

■ REFERENCES

(1) (a) Whitesides, G. M.; Grzybowski, B. *Science* **2002**, *295*, 2418−2421. (b) Tanaka, S.; Kerfeld, C. A.; Sawaya, M. R.; Cai, F.; Heinhorst, S.; Cannon, G. C.; Yeates, T. O. *Science* **2008**, *319*, 1083−1086. (c) Bangham, A. D.; Horne, R. W. *J. Mol. Biol.* **1964**, *8*, 660−668.

(2) (a) Kang, L.; Fu, H.; Cao, X.; Shi, Q.; Yao, J. *J. Am. Chem. Soc.* **2011**, *133*, 1895−1901. (b) Lin, Z.-Q.; Sun, P.-J.; Tay, Y.-Y.; Liang, J.; Liu, Y.; Shi, N.-E.; Xie, L.-H.; Yi, M.-D.; Qian, Y.; Fan, Q.-L.; Zhang, H.; Hng, H. H.; Ma, J.; Zhang, Q.; Huang, W. *ACS Nano* **2012**, *6*, 5309−5319. (c) Liu, H.; Cao, X.; Wu, Y.; Liao, Q.; Jiménez, Á. J.; Würthner, F.; Fu, H. *Chem. Commun.* **2014**, *50*, 4620−4623.

(3) (a) Ghadiri, M. R.; Granja, J. R.; Milligan, R. A.; McRee, D. E.; Khazanovich, N. *Nature* **1993**, *366*, 324−327. (b) Hartgerink, J. D.; Beniash, E.; Stupp, S. I. *Science* **2001**, *294*, 1684−1688. (c) Reches, M.; Gazit, E. *Science* **2003**, *300*, 625−627. (d) Jayawarna, V.; Ali, M.; Jowitt, T. A.; Miller, A. F.; Saiani, A.; Gough, J. E.; Ulijn, R. V. *Adv. Mater.* **2006**, *18*, 611−614. (e) Matsuura, K. *RSC Adv.* **2014**, *4*, 2942−2953.

(4) Ramachandran, G. N.; Ramakrishnan, C.; Sasisekharan, V. *J. Mol. Biol.* **1963**, *7*, 95−99.

(5) (a) Martinek, T. A.; Hetényi, A.; Fülöp, L.; Mándity, I. M.; Tóth, G. K.; Dékány, I.; Fülöp, F. *Angew. Chem., Int. Ed.* **2006**, *45*, 2396−2400. (b) Pomerantz, W. C.; Yuwono, V. M.; Drake, R.; Hartgerink, J. D.; Abbott, N. L.; Gellman, S. H. *J. Am. Chem. Soc.* **2011**, *133*, 13604−13613. (c) Seebach, D.; Gardiner, J. *Acc. Chem. Res.* **2008**, *41*, 1366−1375.

(6) (a) Müller, M. M.; Windsor, M. A.; Pomerantz, W. C.; Gellman, S. H.; Hilvert, D. *Angew. Chem., Int. Ed.* **2009**, *48*, 922−925. (b) Wang, P. S. P.; Nguyen, J. B.; Schepartz, A. *J. Am. Chem. Soc.* **2014**, *136*, 6810−6813.

(7) (a) Kwon, S.; Jeon, A.; Yoo, S. H.; Chung, I. S.; Lee, H.-S. *Angew. Chem., Int. Ed.* **2010**, *49*, 8232−8236. (b) Kwon, S.; Shin, H. S.; Gong, J.; Eom, J.-H.; Jeon, A.; Yoo, S. H.; Chung, I. S.; Cho, S. J.; Lee, H.-S. *J. Am. Chem. Soc.* **2011**, *133*, 17618−17621. (c) Kim, J.; Kwon, S.; Kim, S. H.; Lee, C.-K.; Lee, J.-H.; Cho, S. J.; Lee, H.-S.; Ihee, H. *J. Am. Chem. Soc.* **2012**, *134*, 20573−20576. (d) Kwon, S.; Kang, K.; Jeon, A.; Park, J. H.; Choi, I. S.; Lee, H.-S. *Tetrahedron* **2012**, *68*, 4368−4373.

(8) (a) Chen, C.-L.; Rosi, N. L. *Angew. Chem., Int. Ed.* **2010**, *49*, 1924−1942. (b) Fujiki, Y.; Tokunaga, N.; Shinkai, S.; Sada, K. *Angew. Chem., Int. Ed.* **2006**, *45*, 4764−4767.

(9) Oaki, Y.; Imai, H. *Cryst. Growth Des.* **2003**, *3*, 711−716.

(10) The single crystal of **1** was obtained from aqueous P123 solution and analyzed to support the validity of the Miller index assignment (Figure S4).

(11) Strickland-Constable, R. F. *Kinetics and Mechanism of Crystallization*; Academic Press: New York, 1968.

(12) (a) Manna, L.; Wang, L. W.; Cingolani, R.; Alivisatos, A. P. *J. Phys. Chem. B* **2005**, *109*, 6183−6192. (b) Xiong, Y.; Xia, Y. *Adv. Mater.* **2007**, *19*, 3385−3391.

(13) Mayo, S. L.; Olafson, B. D.; Goddard, W. A. *J. Phys. Chem.* **1990**, *94*, 8897−8909.

(14) Rappé, A. K.; Goddard, W. A. *J. Phys. Chem.* **1991**, *95*, 3358−3363.

(15) Levitt, M.; Hirshberg, M.; Sharon, R.; Laidig, K. E.; Daggett, V. *J. Phys. Chem. B* **1997**, *101*, 5051−5061.

(16) Read, C. G.; Steinmiller, E. M. P.; Choi, K.-S. *J. Am. Chem. Soc.* **2009**, *131*, 12040−12041.

(17) The facet-selective deposition of Pt NPs on $\mathbf{F_2}$ provided similar results with the case of Au (Figure S9).

(18) Yoon, I.; Kang, T.; Choi, W.; Kim, J.; Yoo, Y.; Joo, S.-W.; Park, Q.-H.; Ihee, H.; Kim, B. *J. Am. Chem. Soc.* **2009**, *131*, 758−762.

(19) Interestingly, we often observed in the SEM images of $\mathbf{F_2}$ that they were further assembled hierarchically without any treatment, which was presumably driven by face-to-face association through interfoldecture hydrogen bonds (Figure S11).

DOI: 10.1021/ja510840v
J. Am. Chem. Soc. 2015, 137, 2159−2162